Evaporation process in histological tissue sections for neutron autoradiography

Natalia M. Espector, Agustina Portu, Gustavo A. Santa Cruz & Gisela Saint Martin

Radiation and Environmental Biophysics

ISSN 0301-634X
Volume 57
Number 2

Radiat Environ Biophys (2018)
57:153-162
DOI 10.1007/s00411-018-0735-8

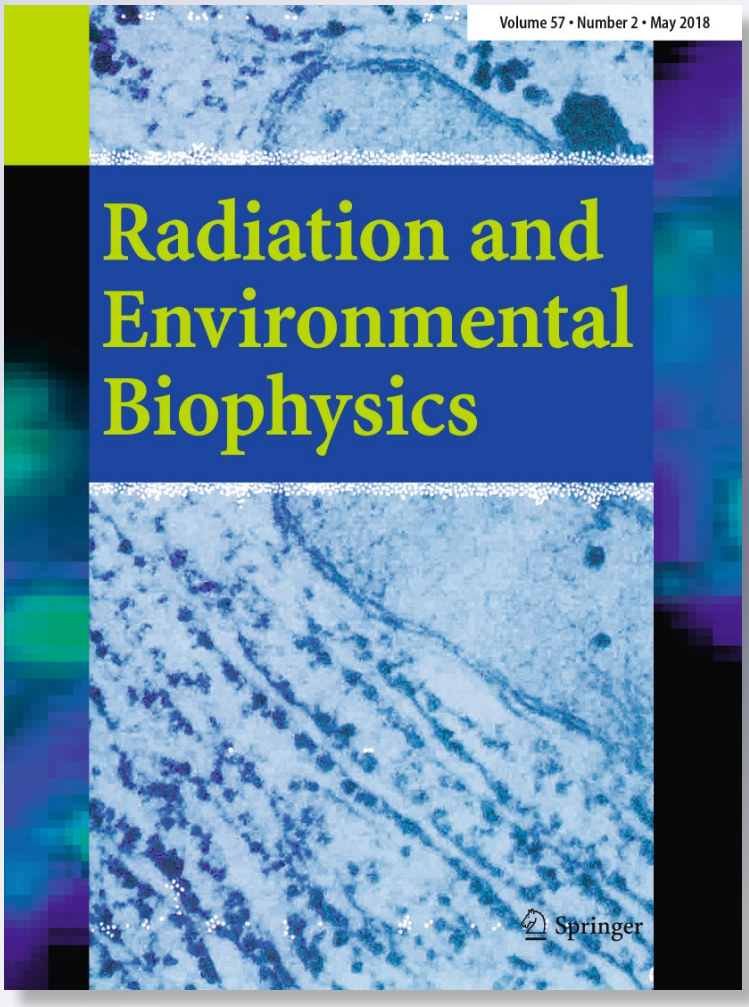

Springer

Radiation and Environmental Biophysics (2018) 57:153–162
https://doi.org/10.1007/s00411-018-0735-8

ORIGINAL ARTICLE

Evaporation process in histological tissue sections for neutron autoradiography

Natalia M. Espector[1,2] · Agustina Portu[3,4] · Gustavo A. Santa Cruz[3] · Gisela Saint Martin[3,5]

Received: 25 July 2017 / Accepted: 19 February 2018 / Published online: 23 February 2018

Abstract

The analysis of the distribution and density of nuclear tracks forming an autoradiography in a nuclear track detector (NTD) allows the determination of ^{10}B atoms concentration and location in tissue samples from Boron Neutron Capture Therapy (BNCT) protocols. This knowledge is of great importance for BNCT dosimetry and treatment planning. Tissue sections studied with this technique are obtained by cryosectioning frozen tissue specimens. After the slicing procedure, the tissue section is put on the NTD and the sample starts drying. The thickness varies from its original value allowing more particles to reach the detector and, as the mass of the sample decreases, the boron concentration in the sample increases. So in order to determine the concentration present in the hydrated tissue, the application of corrective coefficients is required. Evaporation mechanisms as well as various factors that could affect the process of mass variation are outlined in this work. Mass evolution for tissue samples coming from BDIX rats was registered with a semimicro analytical scale and measurements were analyzed with software developed to that end. Ambient conditions were simultaneously recorded, obtaining reproducible evaporation curves. Mathematical models found in the literature were applied for the first time to this type of samples and the best fit of the experimental data was determined. The correlation coefficients and the variability of the parameters were evaluated, pointing to Page's model as the one that best represented the evaporation curves. These studies will contribute to a more precise assessment of boron concentration in tissue samples by the Neutron Autoradiography technique.

Keywords Evaporation dynamics · Cryosectioning · Neutron autoradiography · BNCT

Introduction

The analysis of distribution and concentration of certain elements in a variety of materials can be achieved using Nuclear Track Detectors (NTD), as long as reaction ionizing products are generated by the element to be assessed (Durrani and Bull 1987). In particular, a mapping of ^{10}B atoms present in a tissue section can be obtained by the neutron autoradiography technique, which provides information of the microdistribution of that element in the sample (Portu et al. 2011). In this case, when samples are exposed to thermal neutrons, ^{10}B atoms undergo a neutron capture nuclear reaction [^{10}B(n,α)^{7}Li], which results in the emission of ionizing charged particles (alpha particle, Li ion) that impact the NTD producing localized sites of damage in the material, or nuclear tracks. They can be observed by optical microscopy after a chemical attack, and the ^{10}B concentration in the original tissue can be evaluated through track density measurements on the NTD.

Tissue sections (~30 µm thickness) studied by this technique are obtained from frozen tissue with a cryostatic microtome (cryosectioning), so that the tissue undergoes an evaporation process until reaching ambient temperature. This fact causes dehydration of the tissue section and its nominal thickness (set at the cryostatic microtome) is different from the actual sample thickness at the moment

✉ Gisela Saint Martin
gisaint@cnea.gov.ar

1 Facultad de Ingeniería, Universidad Favaloro, Buenos Aires, Argentina

2 Comisión de Investigaciones Científicas de la Pcia. de Buenos Aires (CIC), Buenos Aires, Argentina

3 Departamento de Radiobiología, Comisión Nacional de Energía Atómica, Av. General Paz 1499, B1650KNA San Martin, Buenos Aires, Argentina

4 Consejo Nacional de Investigaciones Científicas y Técnicas (CONICET), Buenos Aires, Argentina

5 Instituto de Tecnología Jorge Sábato, UNSAM, Buenos Aires, Argentina

of irradiation with thermal neutrons. This process changes the number of particles reaching the detector (which is also related to ions ranges in tissue), thus affecting the determination of boron amount in tissue (Thellier et al. 1988). Moreover, mass variation in the sample impacts directly on the boron concentration value. As a consequence certain correction factors must be applied to take into account this effect (evaporation coefficients, CEv). Since evaporation involves a weight loss in the sample, and assuming that the total boron atoms number remains constant in the process, the evaporation coefficient can be defined as:

$$\mathrm{CEv} = {}^{m_s}\!/_{m_h}, \tag{1}$$

where m_h is the mass of the "wet" tissue section, immediately after being cut with the cryostat, and m_s is the mass of the "dry" sample, at the end of the evaporation process (Gadan et al. 2012).

To understand the evaporation phenomenon, the simplest case is that of a liquid in a gas–vapor mixture. The liquid molecules are in thermal agitation within a wide range of velocities, but for evaporation to occur their kinetic energy must exceed the cohesion work exerted by the surface tension at the liquid outermost layer. So, those molecules with sufficient energy to overcome the intermolecular attraction forces will leave the liquid phase entering the gaseous medium, where they spread out by diffusion. Collisions between molecules could cause some of them to return to the liquid phase and to be reabsorbed. The loss of the faster molecules causes a decrease of the average kinetic energy of molecules in the liquid, lowering its surface temperature (Rolle 2006). This phenomenon is known as evaporative cooling.

Semisolid materials, such as vegetable and animal tissues, could be considered as a three-dimensional solid matrix that contains an aqueous solution. In this case, drying also consists of water changing from the liquid form in the tissue to the vapor phase in the air layer closer to its surface, and the difference of water-free energy in those states commands the process. However, the difference between the two values of free energy decreases throughout the entire process, leading to nonlinear drying kinetics (Pammenter et al. 2002).

Different conditions, which are generally difficult to quantify as they change along the drying period, may determine the evaporation rate. The diffusion of water from the inner part of the tissue to the air is affected by both internal and external factors. For instance, there are retarding resistances in the air layer in contact with the tissue surface, but also in the outermost layer of the tissue itself, depending on its composition and permeability. Also the constraints in the movement of water molecules from the inner part of the tissue to the surface may vary in the process of dehydration.

Mechanisms such as pressure and moisture concentration gradients, capillary forces, effusion, etc. make water cross the material to finally break through the pores and diffuse into the air. The conditions in which the process is carried out necessarily impact on many (physicochemical as well as structural) properties of tissue in a complex way (Skogseth et al. 2014). Volume as well as size and shape of semisolid systems are defined by the particular structure and the mechanical properties of its elements at equilibrium, so water removal from the material implies the rupture of this equilibrium, internal and external pressures are no longer balanced, and contractile stresses are generated causing shrinkage or collapse of the tissue (Mayor and Sereno 2004).

From the mass transport point of view, drying could be understood as a diffusion process. During the first period of drying, the water contained in the material evaporates from its surface to the air flow (by external diffusion). After the moisture gradient inside the material builds up, the second drying period begins. During this period water is transported from the inner part of the material to the surface (internal diffusion) (Chen 2007).Typical drying curves exhibit two stages (Gekas 1992), though there is a previous "warm-up" period that may be relatively short and sometimes can go unnoticed. The first drying stage is known as the "constant rate" period because it shows a linear decrease of water content, the drying rate depending on temperature, moisture and flow of air. The temperature of the material stays constant, i.e. any added heat is consumed to evaporate the free water. The second stage, called "falling rate" period, begins as the passage of internal moisture within the tissue to the surface rules the drying process. The drying rate starts decreasing. The temperature of the material rises causing the mass to decrease. The variation of temperature also produces a diminution of the heat transfer driving forces. The path of evaporated vapors is more complex, so the resistance against the diffusion is higher. During the first part of this period liquid and vapor diffusion through tissue and capillary flow are the proposed mechanisms, and under certain conditions water loss follows a simple negative exponential function, which depends on the drying rate. But when tissue is closer to reach equilibrium with air, the water content diminution is slower (Pinto and Tobinaga 2007; Chen and Peng 2005). Models based on Fick's law are typically used to describe the drying kinetics in the falling rate period (Chen 2007). This law is given by a differential equation describing diffusion of molecules in a medium with concentration or temperature gradients. Here flow of particles or heat tends to homogenize the solution and achieve the chemical or thermal equilibrium. In many cases these models are not able to represent the complexity of the whole process. For example, in tissues

with high water content, the reduction in volume or "shrinkage" (Katekawa and Silva 2006) occurs simultaneously with the diffusion of moisture in the solid, which probably affects the rate of moisture removal.

These models are very complex, and an overall solution to these problems can only be obtained by numerical calculation (Chen 2006; Lu et al. 2015). From this it follows that the question of evaporation involves a large number of mechanisms and factors that may hinder the description of the phenomenon and its resolution. As a rule it is observed that if the drying of the material is "slow" (Pammenter et al. 2002), or under constant relative humidity and temperature (Sun 2002), it can be described by an exponential relationship.

Summarizing, the drying rate of a tissue is affected by factors related to both the particular sample under consideration (amount of material, size and shape, composition of the outermost layer or permeability), and environmental conditions such as air vapor pressure, temperature, and convective air flow on the tissue surface (Esther et al. 2016).

In this work we studied the dynamics of evaporation of thin tissue sections by analyzing sample weight variation. For that purpose a code was designed to record, visualize and analyze data, and a measurement protocol was established, in which local ambient parameters as temperature, pressure and humidity were also considered, as they could affect the evaporation process. Experimental evaporation curves were analyzed through different drying models from the literature, and the influence of sample geometrical characteristics was evaluated.

Materials and methods

Biological material

Tissue sections were obtained using a cryostat microtome Leica Microsystems CM 1850, in the same way they are performed for routine pathological analysis and for the autoradiography technique. The tissue block is fixed to a plate inside the equipment at an established temperature (− 16 or − 18 °C), controlled by thermocouples. For the evaporation analysis, the tissue sections are mounted on 250 μm thickness Lexan™ polycarbonate foils, in order to reproduce the conditions in which neutron autoradiography is performed (e.g., Portu et al. 2013).Normal liver and lung sections from adult BDIX rats (Charles River Lab., MA, USA) were used in these experiments. All samples come from preclinical protocols of other research groups in BNCT (e.g., Garabalino et al. 2011), approved by the Ethics Committee of the Argentine National Atomic Energy Commission. No animals were sacrificed specifically for this study.

Mass measurements

Mass was recorded in a semi micro analytical laboratory scale Sartorius Cubis® Model MSE125P-000-DU-00 ($\sigma_{ap} = 10^{-5}$ g), connected to a PC via a USB port. Typical mass values are $m_h = 0.00150$ g, $m_s = 0.00030$ g.

Taking into account that ambient conditions can affect evaporation mechanisms as well as mass registration (Peña Pérez and Becerra Santiago 2010), the need of recording these factors at the moment of mass registration was considered. INGKA® sensors connected to the PC through a USB port were used to track temporal evolution of pressure, temperature and humidity. Values were acquired every 1 s. The same sampling rate was used for mass recording. The sensors accuracies are: 0.1 °C for the temperature, 0.01 hPa for pressure and 10^{-6}% RH for humidity.

A Graphical User Interface in Matlab was developed for data acquisition and analysis of the results. The program EVAP v.1.0, not only allows recording of data, but also plots the evolution of sample weight in real time, and calculates the evaporation coefficient. Temperature, pressure and humidity files corresponding to the same acquisition period are also read in order to make mass data corrections. A protocol of procedures for data acquisition was established, so as to assure that measurements are always made under the same conditions (Espector et al. 2016).

Mathematical models

Fourteen mathematical models for biological matrices proposed in the literature (Akpinar et al. 2003; Gunhan et al. 2005; Jayas et al. 1991) were evaluated, through the fitting of the experimental data. The equations corresponding to the different models are shown in Table 1.

To compare the curves, the relative mass M_R is defined, which avoids the dependence on the particular values of m_h and m_s as:

$$M_R = \frac{m_i - m_s}{m_h - m_s}, \tag{2}$$

where the mass in the ith instant is represented by m_i. A number of statistical parameters that account for adjustment quality are proposed in the literature (Gunhan et al. 2005; Núñez-Mancilla et al. 2011; Chapra 2012).

In this work we use the Coefficient of determination R^2 (Eq. 3), the mean bias error (MBE) (Eq. 4), the root-mean-square error (RMSE) (Eq. 5), and the reduced Chi-square (Eq. 6):

$$R^2 = 1 - \frac{\sum_{i=1}^{N} \left(M_{R_i} - M_{R_{est,i}}\right)^2}{\sum_{i=1}^{N} \left(M_{R_i} - \bar{M}_{R_i}\right)^2}, \tag{3}$$

Table 1 Mathematical models of mass loss as a function of time (modified from Gunhan et al. 2005)

Model name	Equation	References
Lewis	$M_R = \exp(-kt)$	Lewis (1921)
Page	$M_R = \exp(-kt^n)$	Page (1949)
Modified Page	$M_R = \exp[-(kt)^n]$	White et al. (1981)
Henderson and Pabis	$M_R = a \times \exp(-kt)$	Henderson and Pabis (1961)
Yagcioglu et al	$M_R = a \times \exp(-kt) + c$	Yagcioglu et al. (1999)
Two-term	$M_R = a \times \exp(-k_0 t) + b \times \exp(-k_1 t)$	Henderson (1974)
Two-term exponential	$M_R = a \times \exp(-kt) + (1 - a) \times \exp(-kat)$	Sharaf-Elden et al. (1980)
Wang and Singh	$M_R = 1 + at + bt^2$	Wang and Singh (1978)
Diffusion approach	$M_R = a \times \exp(-kt) + (1 - a) \times \exp(-kbt)$	Kassem (1998)
Verma et al	$M_R = a \times \exp(-kt) + (1 - a) \times \exp(-gt)$	Verma et al. (1985)
Modified Henderson and Pabis	$M_R = a \times \exp(-kt) + b \times \exp(-gt) + c \times \exp(-ht)$	Karathanos (1999)
Simplified Fick's diffusion equation	$M_R = a \times \exp[-c(t/L^2)]$	Diamante and Munro (1991)
Modified Page equation-II	$M_R = a \times \exp[-k(t/L^2)^n]$	Diamante and Munro (1993)
Midilli and Kucuk	$M_R = a \times \exp(-kt^n) + bt$	Midilli et al. (2002)

M_{R_i} is the relative mass experimentally obtained for the ith moment, $M_{R_{est,i}}$ is the estimated relative mass for that instant and N is the total number of experimental data.

$$\mathrm{MBE} = \frac{1}{N}\sum_{i=1}^{N}(M_{R_i} - M_{R_{est,i}}) \tag{4}$$

$$\mathrm{RMSE} = \sqrt{\frac{1}{N}\sum_{i=1}^{N}(M_{R_{est,i}} - M_{R_i})^2} \tag{5}$$

$$\chi^2 = \frac{\sum_{i=1}^{N}(M_{R_i} - M_{R_{est,i}})^2}{N - n} \tag{6}$$

In Eq. 6, n is the number of constants used in the model.

A routine that fits the experimental data with the models proposed in Table 1 was developed. It determines the adjustment parameters for each of the models by the method of least squares. In addition, the statistical parameters defined above are tested.

Geometrical considerations

Reduction in the sample thickness due to evaporation could be approximated by mass loss whenever the tissue section area is assumed to remain unchanged during the evaporation process. While this supposition had been accepted in other works (Thellier et al. 1988; Bortolussi and Altieri 2013) its experimental validation has been accomplished only in this study. For that purpose, different 30 µm thick rat liver sections were mounted on glass and observed in an Olympus DP70 microscope in sequential capture mode. To visualize the effect of dehydration on their area, the tissue sections were photographed sequentially as a whole at low magnification (1.25×), in black and white, starting just after being obtained at the cryostat ("time 0").

In order to assess the impact of the tissue section area on the dynamics of evaporation, a set of BDIX rat liver sections were measured. The first ones were taken from a tissue block (area A1), then the block was reduced in size with a scalpel twice (areas A2 and A3) and the other sections were obtained. In all cases, the nominal section thickness was 30 µm. Evaporation curves of the tissue sections were registered.

Drying curve dependence on section thickness was also studied. With that purpose, BDIX rat liver sections of 5, 10, 20, 30 and 60 µm nominal thicknesses were performed. Moreover, the influence of thickness in the evaporation dynamics was also studied through a series of experiments using an infrared thermal imaging camera. Dynamic Infrared Thermography is a non-invasive technique that determines the temperature distribution of an observed "scene" during time, by recording the infrared radiance coming from that scene and converting it to temperature. For this experiment, sections of BDIX rat liver of 10, 30 and 60 µm thicknesses were used. Mass variation was recorded simultaneously with Infrared Thermography images of samples acquired sequentially, in each case. A FLIR model T-420 camera was used, which achieves a spatial resolution of 100 µm, 50 mK temperature sensitivity, working range from −20 to 650 °C, and acquisition of radiometric images and videos at 30 Hz rate. An area of 3 × 3 pixels at the center of the tissue section was selected in each video and the temperature data as a function of time of that particular area were recorded through specific software.

Results and discussion

Considering the nominal appreciation of the scale and calculating the relative errors for typical mass values ($m_h = 0.00150$ g, $m_s = 0.00030$ g), an uncertainty of 5% in the expression of mass ratios was obtained (and for the CEv in particular) for this method.

It was observed that all the measurements of tissue weights were stabilized in about 5 min or less. So an average value of readings in the time range from 0.1 to 0.2 h (6–12 min) was used to determine the stabilization mass m_s, since once the evaporation process is complete readings scarcely fluctuate around a midline.

Certain relationships between ambient conditions and changes in the mass readings had been found previously. Two correction factors could be determined in order to reduce the uncertainty associated with the scale drift over time and obtain stable readings (Espector 2016).

Regarding to possible variation of the tissue section area while drying, the images of the whole set of sequential photographs were digitally superimposed finding that the area remained unchanged within the accuracy of the procedure (data not shown). Images of several tissue sections were taken after some months of being sliced, and no difference was observed. In summary it could be concluded that the most important tissue section reduction occurs most noticeably by changes in its thickness.

The complexity of the evaporation process in tissues, that has been outlined in the Introduction, makes it extremely difficult to set up a mechanistic model of the phenomenon, and more simple presumptions can be made. In fact, in the case of our samples, an external air flow is not applied and evaporation occurs at room temperature. Moreover no significant fluctuations of this variable occur during the measurement (in general, differences do not exceed 0.3 °C).

In this work BDIX rats liver sections were considered to test the models presented in Table 1, which are generally expressed by negative exponential functions. Thirteen curves of mass evolution were registered for sections corresponding to this type of tissue, as seen in Fig. 1. The measurements correspond to sections coming from the same animal, but (1) taken at different times of day, (2) different days, (3) same block of tissue that remained in the cryostat, (4) different tissue blocks. In order to compare results, the mass values at the ith instant are normalized to the first value (Evap $= m_i/m_h$). The final mass normalized value remained reproducible even varying the experimental conditions in which the sections were obtained. The CEv for these curves was 0.31 ± 0.02 (mean $\pm$ standard deviation), which matches with a historical value determined by thermogravimetry (Portu et al. 2015).

A preliminary comparison of the R^2 coefficients led to a first selection, such that those curves with a value of less than 0.96 were discarded. In this way the analysis was reduced to three models: Page, Henderson and Pabis and Yagcioglu.

These models are all exponentially decreasing equations with different variants and also yielded satisfactory results for the other statistical parameters that account for adjustment quality (Table 2).

Figure 2 shows results obtained from adjusting the average liver evaporation curve with the three selected models.

Table 2 Statistical parameters calculated for Page, Henderson and Pabis and Yagcioglu curves

	R^2	SSE	RMSE	Chi
Page	0.9686	− 0.0045	0.0434	0.0019
Henderson and Pabis	0.9642	− 0.0066	0.0463	0.0021
Yagcioglu	0.9655	− 1.88E−09	0.0455	0.0021

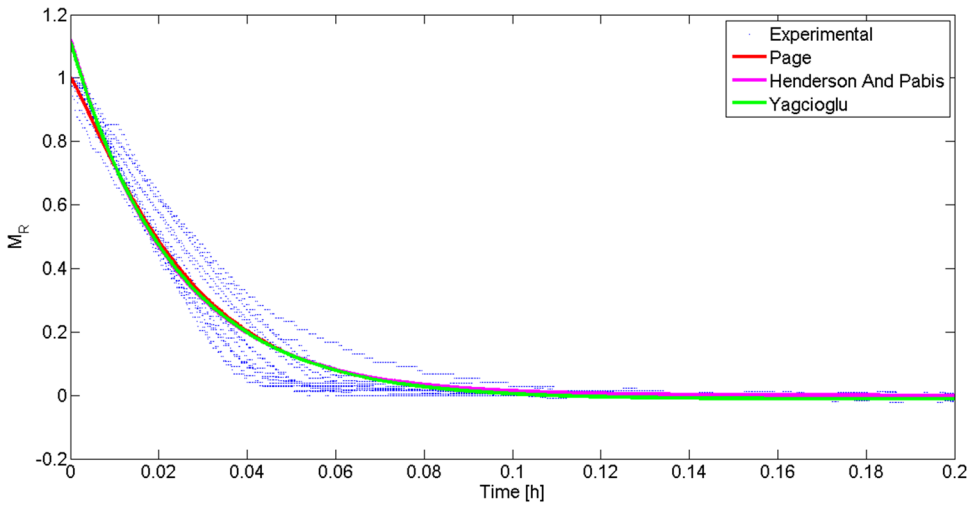

Fig. 1 Mass evolution registered for sections corresponding to BDIX rats liver. Curve fitting with Page, Henderson and Pabis and Yagcioglu equations

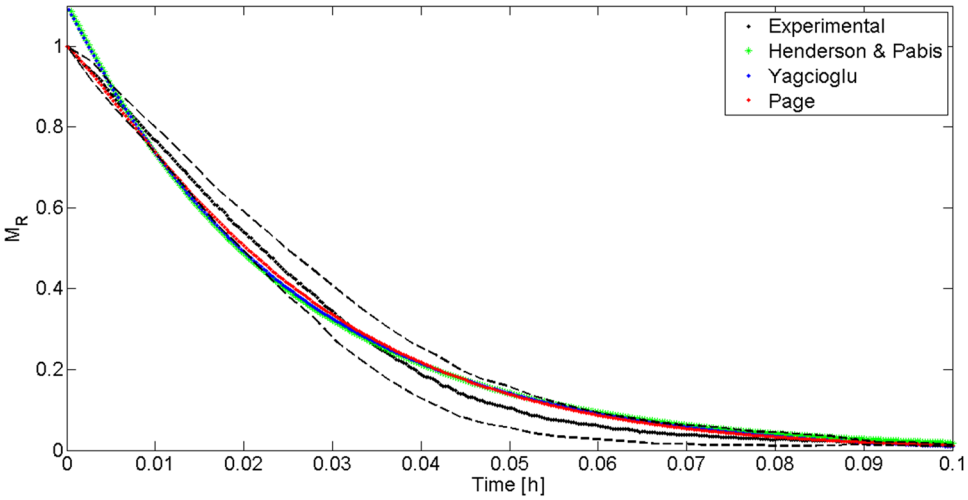

Fig. 2 Average evaporation curve of BDIX rat liver sections, fitted with the three selected models. The black full line corresponds to the average of all the considered experimental curves and the standard deviation is represented in dotted lines

Though they are quite similar almost for all the registered times, the fit obtained with the Page model keeps always within the zone determined by the average experimental curve and the curves generated from the standard deviation. Furthermore, the calculated value with this model at time 0 is 1, which is consistent with the fact that normalized values are being considered.

About 70 mass versus time evolution curves including various experimental conditions and different tissues from diverse animal species were also tested with the models. Data corresponding to 16 BDIX rat lung sections were also fitted and the resulting curves exhibited the same behavior as those corresponding to normal liver.

Finally experimental curves were analyzed individually. The variation of the adjustment parameters corresponding to each of the three models was analyzed, considering that parameters from curves from the same type of tissue and registered under similar experimental conditions should be alike. The results of this analysis are shown in Table 3 that also includes measurements from BDIX rat lung sections. The smallest deviations of the adjustment parameters were obtained for the Page model.

The Yagcioglu model could also be discarded following a principle of simplicity, since it contains three adjustment parameters instead of two. This fact explains the high deviations found for these constants. Furthermore, the fact that a single set of parameters cannot be assigned to a family of curves makes it difficult to attribute a physical meaning to them.

So, even though the three models could be acceptable regarding to the statistical parameters results, Page's model appears to be the best description of this particular problem.

Curves of weight loss for tissue sections of different area and equal thickness are shown in Fig. 3. It can be seen that the larger the section area, the longer the stabilization time. At least for the tested areas, the period used to calculate the dry mass m_s remains valid. However, this time interval should be revised in case the mass is much higher than those used in this study. It should be noticed that the tissue sections commonly used in practice for neutron autoradiography have areas in the range between those of samples A2 and A3, i.e. masses below 2.5 mg. Data corresponding to the three areas were adjusted using the Page model. The parameter k was found to keep almost the same in all cases. On the other hand, parameter n was 20% (for A1) and 12% (for A2) higher than the one obtained for A3. Thus it could be inferred that parameter n increases with tissue section area. In spite of the dependence of the evaporation dynamics on the tissue area, the results obtained for the CEv matched each other.

Table 3 Mean adjustment parameters and their standard deviation (SD) for the three analyzed models, corresponding to experimental data from BDIX rat liver and lung slices

Model	Parameter	BDIX rat liver	BDIX rat lung
Page $M_R = \exp(-kt^n)$	$<k>$	63	63
	SD k	5%	6%
	$<n>$	1.16	1.13
	SD n	6%	8%
Henderson and Pabis $M_R = a \times \exp(-kt)$	$<a>$	1.13	1.10
	SD a	3%	4%
	$<k>$	43	46
	SD k	21%	26%
Yagcioglu $M_R = a \times \exp(-kt) + c$	$<a>$	1.1	1.1
	SD a	3%	4%
	$<k>$	− 0.02	− 0.01
	SD k	89%	77%
	$<c>$	41	45
	SD c	24%	29%

SD values higher than 10% are underlined

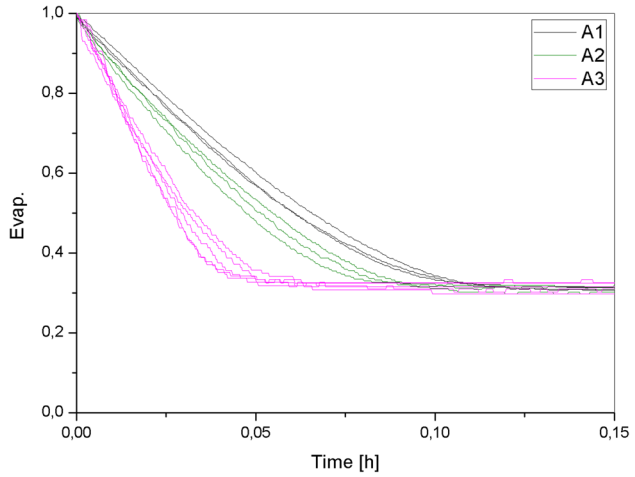

Fig. 3 Evaporation dynamics of 30 µm thickness sections with different areas (BDIX rat liver). The area is classified by its initial mass m_h. $m_{A1} = 3.8 \pm 0.1$ mg, $m_{A2} = 2.5 \pm 0.1$ mg, and $m_{A3} = 1.1 \pm 0.1$ mg

In Fig. 4 evaporation curves for tissue sections of the same area and different thicknesses are shown. As expected, the larger the section thickness, the slower the stabilization process. However, this parameter does not affect the CEv final value. These results confirm the dependence of evaporation dynamics with tissue geometry: a greater thickness causes that water molecules in the tissue take longer to diffuse and reach the surface. Water molecules inside the tissue must travel a distance to reach the surface and evaporate, and as the tissue is thicker, the path is longer.

Evaporation curves corresponding to sections of different thicknesses were also fitted with Page's model and the obtained parameters k and n were analyzed. The results of this study are plotted in Fig. 5.

In this case, as in the previous experience, parameter k remains unchanged. On the other hand a relationship between n and the section thickness (and therefore with the time necessary to achieve stabilization) could be established. The results of these tests suggest that although the Page model has two adjustable parameters, only one of them is sensitive to the geometric variations imposed in the experiments. Thus it could also be associated to the speed necessary for the sample mass to stabilize. Parameter n was plotted as a function of the sample mass (which as it was mentioned, accounts for the area) and as a function of the section thickness (Fig. 6).

As mentioned before no variations were found in parameter k under the different experimental conditions. It could be considered as a constant, at least within the conditions in which the measurements were realized. It should be remarked that although parameter n is related to the evaporation dynamics, the final result of CEv showed no dependence on any of the two parameters of the model.

Gunhan et al. (2005) established that parameters k and n were related to environmental conditions, and in particular they determined that k depended on temperature and relative humidity. It is important to note that in the above mentioned work, experiments were carried out over a wide range of temperature (40, 50 and 60 °C) and relative humidity (5, 15 and 25%) variation. However, measurements carried out in the present study were made at laboratory temperature, humidity and pressure, so that changes of the different variables were not significant, even though they have been performed in different seasons of the year. This could be the reason why values found for k are practically constant.

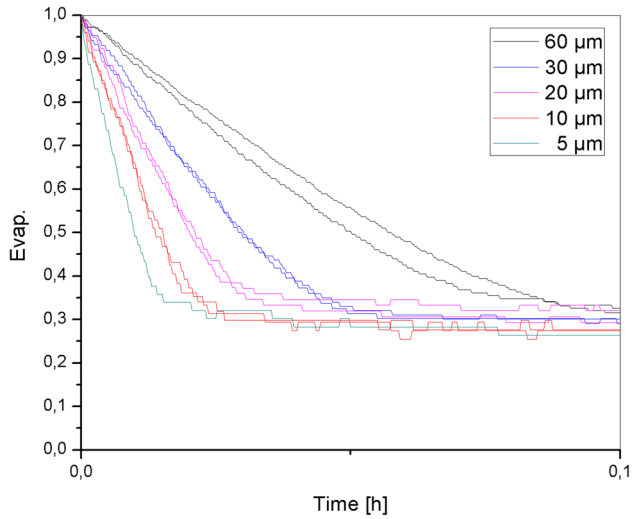

Fig. 4 Mass variation as a function of time for liver samples of different thicknesses coming from BDIX rats

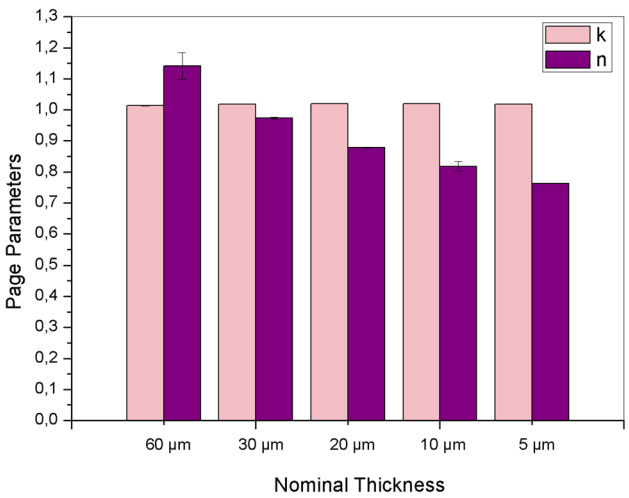

Fig. 5 Average normalized k and n parameters obtained from fitting the data with the Page model, for different slice nominal thickness

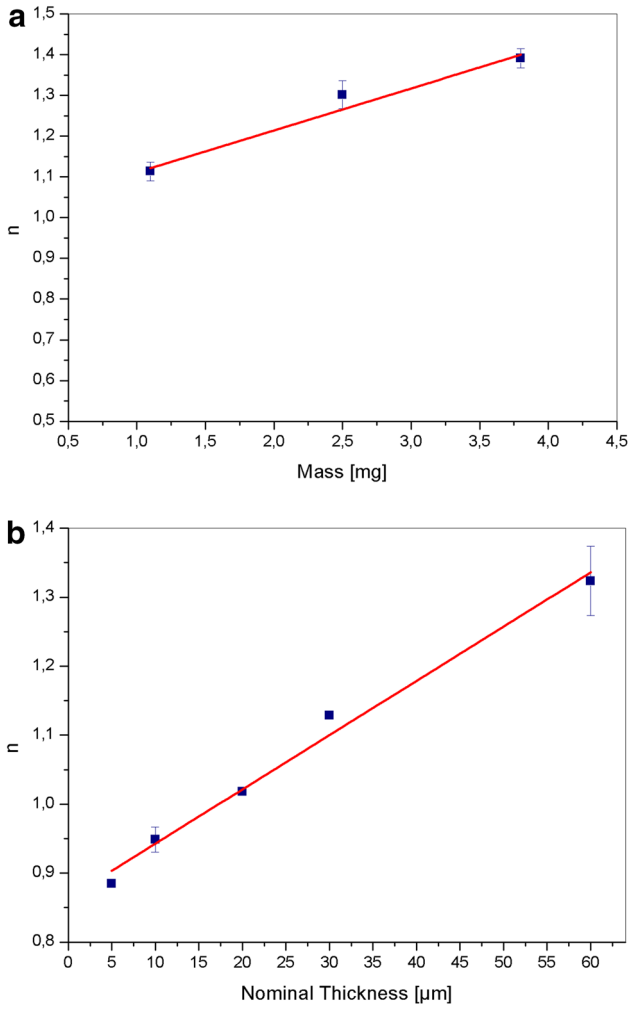

Fig. 6 Variation of parameter n (Page model) as a function of **a** sample mass (which accounts for the area) and **b** thickness. The experimental data could be fitted by the equations $n = 0.10 \times [\text{mass}] + 1.01$ and $n = 0.0079 \times [\text{thickness}] + 0.86$, with $R^2 = 0.96$ and $R^2 = 0.98$, respectively

In relation to measurements of sample temperature made by Thermography, the obtained curves are shown in Fig. 7, along with those corresponding to simultaneous measurements of mass during the evaporation process. The three curves related to samples of different thickness (10, 30 and 60 μm) have two transients in which the temperature increases, and two ranges in which it remains constant. In the mass evolution curves, it can be observed that the values stabilize at the beginning of the second transient. While evaporation occurs, the mass varies and the temperature remains constant (i.e., the temperature remains constant during a phase change; the heat transferred to the liquid water in the tissue is used up in its change of state and does not influence the tissue temperature). The first transient, probably due to its short time length, goes unnoticed in the curves of mass evolution and could be related to the constant rate period described in the Introduction.

It was also observed in the video sequence acquired by the thermal camera that the temperature changes in the tissue section are not uniform, but occur from the edges of the sample towards the center. This can be associated with the differences in stabilization velocity observed in sections of different area (Fig. 7): a larger surface implies that the evaporation process will be slower.

Another result obtained from measurements made by Infrared Thermography is related to the fact that stabilization time was determined more precisely, and a proportionality ratio between this value and the tissue section thickness was found. Thus, at least in the studied thickness range, it was proposed that:

$$t_{\text{estab}_j} \approx \frac{e_j}{e_i} t_{\text{estab}_i}, \tag{7}$$

where t_{estab} is the stabilization time and e is the thickness of the tissue section, for any pair of cases i, j within the range of this study. In this way, it would be possible to estimate the time necessary to stabilize for a tissue section of a given thickness, and the interval along which the dry mass m_s should be calculated.

In spite of differences found in relation to the evaporation dynamics, the final CEv proved to be independent of the nominal section thickness and area. This finding is of great relevance for samples in which the mass is too small, where larger errors are introduced in the measurement. In these cases, sections of greater thickness than usual could be made, in order to obtain an initial mass of greater magnitude. It should be noted that increasing the thickness also implies an increase in the stabilization time, so it may be necessary to modify the time period considered to calculate the dry mass m_s, for which Eq. 7 would be useful.

Conclusions

A protocol was established in order to study evaporation in thin tissue sections by measuring mass variation. An analysis of drying curves corresponding to models found in the literature was done, based on the comparison of various statistical parameters. The best fit of the experimental data of sample weight as a function of time was obtained with the curve proposed in the Page model. Although this equation has two adjustable parameters, only one of them showed a dependence on geometric characteristics of the tissue section (area, thickness).

It was found that the ambient parameters did not affect the results, as long as the measurements are carried out under normal ambient conditions. However, as future work,

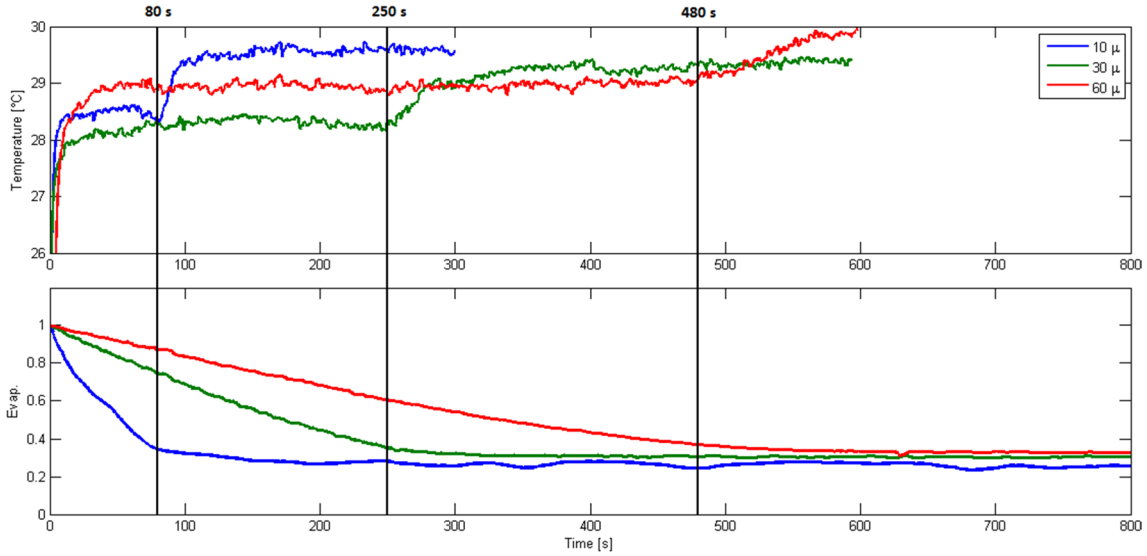

Fig. 7 Temperature curves of three BDIX rat liver sections of different thicknesses measured by infrared thermography (upper panel) and their corresponding evaporation registers (lower panel). The moments in which the second transient begins for each thickness, are indicated with black vertical lines

a broader analysis is proposed to study the influence of environmental conditions on the adjustment parameters and eventually find a functional relationship between these parameters and the environmental and geometric variables. The fact that experimental results could be adjusted with Page's equation opens the possibility of using the selected model to predict the mass change, especially in those cases where the scale measurement is difficult.

As expected, the tissue section thickness has a direct influence on the time the mass needs to reach stabilization. On the other hand for the range of areas of interest, the effect of the tissue section area on the stabilization time is of no importance, but it should be taken into account in case of using larger tissue blocks.

Measurements by Infrared Thermography showed that mass loss during the evaporation process occurs at constant temperature of the sample. The different evaporation stages described in the theory were observed and a proportionality relationship between the thickness of the tissue section and the stabilization time was proposed at least for the considered thicknesses range.

This work also allowed the assessment of CEv under similar conditions to those routinely used for boron concentration determination in tissue samples through the neutron autoradiography technique. This study has proved that although parameters in Page's model are related to the evaporation dynamics the final result of CEv showed no dependence on any of them, which reflects the fact that neither geometrical nor ambient factors affect the CEv values. This work, that has extensively studied the influence of those factors on the evaporation process in tissue sections, would allow us to infer that CEv's mainly depend on the particular type of tissue.

Acknowledgements The authors want to thank to Dr. A. Schwint and co-workers for providing biological samples. This work was partially supported by a Grant from Alberto J. Roemmers Foundation.

References

Akpinar E, Midilli A, Bicer Y (2003) Single layer drying behaviour of potato slices in a convective cyclone dryer and mathematical modeling. Energy Convers Manag 44:1689–1705

Bortolussi S, Altieri S (2013) Boron concentration measurement in biological tissues by charged particle spectrometry. Radiat Environ Biophys 52:493–503

Chapra SC (2012) Applied numerical methods with MATLAB for engineers and scientists, 3rd edn. McGraw-Hill, New York

Chen X (2006) Guest editorial. Dry Technol 24:121–122

Chen X (2007) Moisture diffusivity in food and biological materials. Dry Technol 25:1203–1213

Chen X, Peng F (2005) Modified biot number in the context of air drying of small moist porous objects. Dry Technol 23:83–103

Diamante LM, Munro PA (1991) Mathematical modelling of hot air drying of sweet potato slices. Int J Food Sci Technol 26:99

Diamante LM, Munro PA (1993) Mathematical modelling of the thin layer solar drying of sweet potato slices. Sol Energy 51:271–276

Durrani SA, Bull RK (1987) Solid state nuclear track detection. Principles, methods and applications. In: terHaar D (ed) International series in natural philosophy. Pergamon Press, Oxford

Espector N (2016) Estudio de la evaporación en cortes histológicos y su efecto en el análisis autorradiográfico de tejidos a tratar con BNCT. Medical Physics Engineering Thesis. Favaloro University, Buenos Aires, Argentina

Espector N, Portu A, Leyva G, Saint Martin G (2016) Evaporation in Tissue Sections used for Neutron Autoradiography in BNCT. In: 17th international neutron capture therapy conference, Missouri

Esther MS, Banuu Priya EP, Subhashini S (2016) Thin layer and deep bed drying basic theories and modelling: a review. AgricEngInt CIGR J 18(1) Open access at http://www.cigrjournal.org

Gadan MA, Bortolussi S, Postuma I, Ballarini F, Bruschi P, Protti N, Santoro D, Stella S, Cansolino L, Clerici A, Ferrari C, Zonta A, Zonta C, Altieri S (2012) Set-up and calibration of a method to measure ^{10}B concentration in biological samples by neutron autoradiography. Nucl Instrum Methods B 274:51–56

Garabalino MA, Monti Hughes A, Molinari AJ, Heber EM, Pozzi ECC, Cardoso JE, Colombo LL, Nievas S, Nigg DW, Aromando RF, Itoiz ME, Trivillin VA, Schwint AE (2011) Boron neutron capture therapy (BNCT) for the treatment of liver metastases: biodistribution studies of boron compounds in an experimental model. Radiat Environ Biophys 50:199–207

Gekas V (1992) Transport phenomena of foods and biological materials. CRC Press, Boca Raton

Gunhan T, Demir V, Hancioglu E, Hepbasli A (2005) Mathematical modeling of drying of bay leaves. Energy Convers Manag 46:1667–1679

Henderson SM (1974) Progress in developing the thin layer drying equation. Trans ASAE 17:1167–1168

Henderson SM, Pabis S (1961) Grain drying theory I. Temperature effect on drying coefficient. J Agric Eng Res 6:169–174

Jayas DS, Cenkowski S, Pabis S, Muir WE (1991) Review of thin-layer drying and wetting equations. Dry Technol 9:551–588

Karathanos VT (1999) Determination of water content of dried fruits by drying kinetics. J Food Eng 39:337–344

Kassem AS (1998) Comparative studies on thin layer drying models for wheat. In: 13th international congress on agricultural engineering, Morocco, vol 6

Katekawa ME, Silva MA (2006) A review of drying models including shrinkage effects. Dry Technol 24:5–20

Lewis WK (1921) The rate of during of solid materials. Ind Eng Chem 13:427

Lu T, Wang HL, Jian PX (2015) A thermo–hydro–mechanics bidirectional coupling mathematical model for drying of biological porous medium. Dry Technol 33:420–428

Mayor L, Sereno AM (2004) Modelling shrinkage during convective drying of food materials: a review. J Food Eng 61:373–386

Midilli A, Kucuk H, Yapar Z (2002) A new model for single layer drying. Dry Technol 20(7):1503–1513

Núñez-Mancilla Y, Perez-Won M, Vega-Gálvez A, Arias V, Tabilo-Munizaga G, Briones-Labarca V, Lemus-Mondaca R, Di Scala K (2011) Modeling mass transfer during osmotic dehydration of strawberries under high hydrostatic pressure conditions. Innov Food Sci Emerg Technol 12:338–343

Page G (1949) Factors influencing the maximum rates of air drying shelled corn in thin layer. Master Thesis. Purdue University

Pammenter NW, Berjak P, Wesley-Smith J, Vander Willinger C (2002) Methods for the study of water relations under desiccation stress. In: Black M, Pritchard HW (eds) Desiccation and survival in plants. CABI Publishing, UK

Peña Pérez LM, Becerra Santiago LO (2010) Impacto de la nueva fórmula de la densidad del aire CIPM-2007. Simposio de metrología. Centro Nacional de Metrología (CENAM), México

Pinto LAA, Tobinaga S (2007) Diffusive model with shrinkage in the thin-layer drying of fish muscles. Dry Technol 24:509–516

Portu A, Carpano M, Dagrosa A, Nievas S, Pozzi E, Thorp S, Cabrini RL, Liberman S, Saint Martin G (2011) Reference systems for the determination of ^{10}B through autoradiography images: application to a melanoma experimental model. Appl Radiat Isot 69:1698–1701

Portu A, Carpano M, Dagrosa A, Cabrini RL, Saint Martin G (2013) Qualitative autoradiography with polycarbonate foils enables histological and track analyses on the same section. Biotech Histochem 88(5):217–221

Portu A, Postuma I, Gadan MA, Saint Martin G, Olivera MS, Altieri S, Protti N, Bortolussi S (2015) Inter-comparison of boron concentration measurements at INFN-University of Pavia (Italy) and CNEA (Argentina). Appl Radiat Isot 105:35–39

Rolle KC (2006) Termodinámica, 6th edn. Ed. Pearson Educación, Mexico

Sharaf-Elden YI, Blaisdell JL, Hamdy MY (1980) A model for ear corn drying. Trans ASAE 23:1261–1265

Skogseth H, Eikvik T, Tvedt K, Strommen I, Larsson E, Halgunset J (2014) Can drying be an alternative tissue preservation method in cancer research biobanking? Dry Technol 32:713–719

Sun WQ (2002) Methods for the study of water relations under dessication stress. In: Black M, Pritchard HW (eds) Desiccation and survival in plants. CABI Publishing, UK

Thellier M, Hennequin E, Heurteaux C, Martini F, Pettersson M, Fernandez T, Wissocq JC (1988) Quantitative estimation in neutron capture radiography. Nucl Instrum Methods Phys Res B 30:567–579

Verma LR, Bucklin RA, Endan JB, Wratten FT (1985) Effects of drying air parameters on rice drying models. Trans ASAE 28:296–301

Wang CY, Singh RP (1978) A single layer drying equation for rough rice. Paper no. 78-3001, American Society of Agricultural Engineers, St. Joseph, MI

White GM, Ross IJ, Ponelert R (1981) Fully exposed drying of popcorn. Trans ASAE 24:466–468

Yagcioglu A, Degirmencioglu A, Cagatay F (1999) Drying characteristic of laurel leaves under different conditions. In: Bascetincelik A (ed) Proceedings of the 7th international congress on agricultural mechanization and energy, Adana, Turkey. Faculty of Agriculture, Cukurova Universty, pp 565–569